Erschienen in: Science China Life Sciences. Springer. 2023, 66(6), pp. 1213-1230
https://doi.org/10.1007/s11427-022-2317-6

The genetic basis of the leafy seadragon's unique camouflage morphology and avenues for its efficient conservation derived from habitat modeling

Meng Qu[1,2,3†], Yingyi Zhang[1,2,3†], Zexia Gao[4†], Zhixin Zhang[1,2,7†], Yali Liu[1,2,3], Shiming Wan[4], Xin Wang[1,2], Haiyan Yu[1,2], Huixian Zhang[1,2], Yuhong Liu[1,2], Ralf Schneider[5], Axel Meyer[6*] & Qiang Lin[1,2,3*]

[1]*CAS Key Laboratory of Tropical Marine Bio-Resources and Ecology, South China Sea Institute of Oceanology, Chinese Academy of Sciences, Southern Marine Science and Engineering Guangdong Laboratory (GML, Guangzhou), Guangzhou 511458, China;*
[2]*Sanya Institute of Oceanology, SCSIO, Sanya 572000, China;*
[3]*University of Chinese Academy of Sciences, Beijing 100049, China;*
[4]*College of Fisheries, Key Lab of Freshwater Animal Breeding, Ministry of Agriculture, Huazhong Agricultural University, Wuhan 430070, China;*
[5]*Marine Evolutionary Ecology, Zoological Institute, Kiel University, 24118 Kiel, Germany;*
[6]*Department of Biology, University of Konstanz, 78464 Konstanz, Germany;*
[7]*Global Ocean and Climate Research Center, South China Sea Institute of Oceanology, Guangzhou 510301, China*

The leafy seadragon certainly is among evolution's most "beautiful and wonderful" species aptly named for its extraordinary camouflage mimicking its coastal seaweed habitat. However, limited information is known about the genetic basis of its phenotypes and conspicuous camouflage. Here, we revealed genomic signatures of rapid evolution and positive selection in core genes related to its camouflage, which allowed us to predict population dynamics for this species. Comparative genomic analysis revealed that seadragons have the smallest olfactory repertoires among all ray-finned fishes, suggesting adaptations to the highly specialized habitat. Other positively selected and rapidly evolving genes that serve in bone development and coloration are highly expressed in the leaf-like appendages, supporting a recent adaptive shift in camouflage appendage formation. Knock-out of *bmp6* results in dysplastic intermuscular bones with a significantly reduced number in zebrafish, implying its important function in bone formation. Global climate change-induced loss of seagrass beds now severely threatens the continued existence of this enigmatic species. The leafy seadragon has a historically small population size likely due to its specific habitat requirements that further exacerbate its vulnerability to climate change. Therefore, taking climate change-induced range shifts into account while developing future protection strategies.

seadragon, camouflage, olfactory receptor, global climate change, habitat suitability, conservation

†Contributed equally to this work
*Corresponding authors (Axel Meyer, email: axel meyer@uni-konstanz de; Qiang Lin, email: linqiang@scsio ac cn)

INTRODUCTION

Charles Darwin famously ended the first edition of the Origin of Species with "from so simple a beginning endless forms most beautiful and most wonderful" (Darwin, 2004). The leafy seadragon *Phycodurus eques* (Günther, 1865) certainly belongs to nature's most extraordinary creatures, because of its many unique biological features and its iconic morphology (Figure 1A). The leafy seadragon is endemic to South Australia's coastal regions, where within this already small distribution, it is further limited to specific habitats of kelp forests and seagrass meadows (Browne et al., 2008), making it vulnerable to local and global environmental changes (Kuiter, 2000; Pollom et al., 2021).

Adorned with gossamer, leaf-shaped appendages covering their bodies, seadragons perfectly blend in with the kelp and seaweeds that they inhabit (Branshaw, 2005). The leafy seadragon is one of Australia's national emblems, as well as a flagship species for the global conservation of marine life. Sadly, the wild leafy seadragon populations are shrinking drastically due to habitat destruction, pollution, and poaching (IUCN, 2020). Moreover, despite its instant recognizability, virtually nothing is known about its population history or the genetic basis of its conspicuous camouflage.

Endemics normally have narrower niches than widespread species and are thus considered more sensitive to environmental changes and suffer higher rates of extinction (Sala et al., 2000). Syngnathids, due to their small clutch sizes, direct development in their fathers' pouches, sedentary life-style and highly specific ecological niches, are especially vulnerable (Connolly et al., 2002; van Wassenbergh et al., 2011). Upright swimming in seahorses and their prehensile tails are associated with the expansion of shallow-water areas and seagrass habitats. Their non-fish-like posture and shape probably also enhance their crypsis without negatively affecting maneuverability, which they manage although they lack caudal and pelvic fins (Teske and Beheregaray, 2009).

Some genetic changes associated with phenotypic adaptations have been identified in some species of seahorses and their relatives. For example, the loss of the limb-related gene *tbx4* in seahorses was demonstrated to affect pelvic fin formation (Lin et al., 2016), and the pseudogenization of the *scpp5* gene was likely responsible for the loss of teeth in syngnathids (Qu et al., 2021). Therefore, the analysis of the leafy seadragon genome could provide a link to explore the evolutionary signatures of the unique phenotypes and a foundation for future conservation strategies.

Climate change is one of the direct drivers of global biodiversity loss (Díaz et al., 2019) and adversely affects many marine species (Lindsey and Dahlman, 2020), leading to shifts in distributions, body size, phenology, and behavior of myriads of organisms (Sheridan and Bickford, 2011). Moreover, climate change-induced range shifts not only directly influence marine organisms but also result in novel species interactions and reduce the protective effect of nature reserves (Dobrowski et al., 2021; Wei et al., 2022). Therefore, to better understand how to conserve seadragons, it is necessary to predict the impact of future climate change on habitat loss and the distribution of this species.

We assembled a *de novo* leafy seadragon genome, and conducted, in order to gain biological insights into this iconic species, further comparative genomic analyses. This study provides insights into the genetic basis for extraordinary camouflage of the leafy seadragon, addressed using the CRISPR-Cas9 methodology. Furthermore, the most simplified but specific olfactory receptors were found in seadragons, suspected to be ecological adaptations to the highly specialized environments of kelp forests and seagrass beds. The historical and contemporary population dynamics were determined and predicted, and species distribution models (SDMs) were developed to predict their potential distribution changes under climate change scenarios (Guisan et al., 2017), and meanwhile, to offer valuable knowledge for guiding long-term conservation of the leafy seadragons.

RESULTS

Comparative genomics and evolutionary rates

The leafy seadragon genome was sequenced from a piece of the leaf-like appendage of an adult male. The final assembly was 871 Mb (N50, 5.95 Mb), with an estimated completeness of approximately 95% in BUSCO scores (Tables S1 and S2 in Supporting Information). This genome was predicted to contain 20,113 protein-coding genes, and a relatively high level of transposable elements (TEs) and other interspersed repeats (~61%) (Figure S1, Tables S3–S6 in Supporting Information). The correlations between genome size and the proportion of TEs across published syngnathids and other representative teleosts were separately calculated. Overall, the relative TE content was positively correlated with genome size in both groups, with a higher correlation coefficient in syngnathids (Figure 1C and Table S7 in Supporting Information). The proportion of retrotransposon short interspersed nuclear elements (SINEs) in the leafy seadragon was found to be significantly higher than that in other syngnathid species (Figure 1D).

Next, we constructed a high-confidence species tree for eight syngnathids and another 13 ray-finned fishes using a genome-wide set of 637 one-to-one orthologous genes. We confirmed that the leafy seadragon is sister to the weedy seadragon (*Phyllopteryx taeniolatus*) and estimated their divergence to have happened during the Neogene—about 9.3 million years ago (Mya) (Figure 1B; Figure S2 in Supporting Information). Previous studies revealed that seahorses have among the highest evolutionary rates of teleosts, suggesting

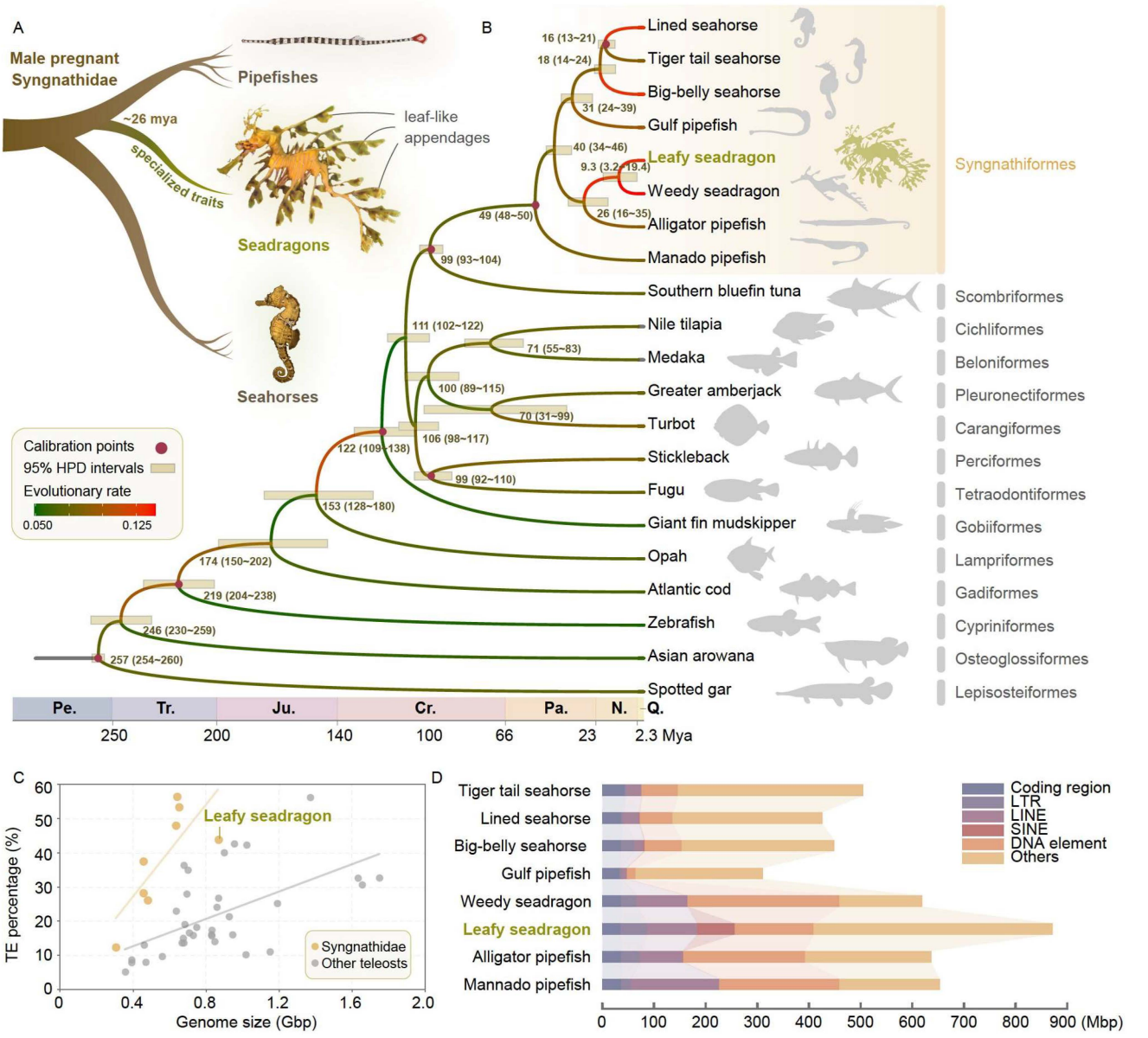

Figure 1 Phylogenetic position and genomic TE characteristics of the leafy seadragon. A, The morphological diversity in Syngnathidae. Seadragons have large body sizes, the dragon-like shape body with dermal appendages. B, Phylogenetic relationships of the leafy seadragon and 20 representative teleosts. The numbers labeled on the tree refer to the estimated divergence time, and the red dots on the shadow rectangle on each node show the 95% confidence interval. Branches are colored based on ω (dN/dS). Pe., Permian; Tr., Triassic; Ju., Jurassic; Cr., Cretaceous; Pa., Paleogene; N., Neogene; Q., Quaternary. C, Correlation between genome size and the proportion of TEs in syngnathids (yellow, r=0.5873, P=0.0266) and representative teleosts (gray, r=0.3230, P=0.0004). Genome size statistics of the leafy seadragon and seven other syngnathid species. D, The diagram indicates the size of each type of element, including the coding regions, LINEs, SINEs, LTRs, DNA elements, and other genomic regions in each species.

that this might be linked to the morphological divergence of their lineage (Lin et al., 2016). By calculating the substitution rates, we found that rapid evolution (0.0020 dS/Mya) originally occurred in the common ancestor of the tail-brooders (subfamily Syngnathinae), whereas in Manado pipefish—the representative of trunk-brooders in the subfamily Nerophinae included in this analysis—the substitution rate was more moderate compared with that of most other teleosts (0.0001–0.0008 dS/Mya, Figure S3 in Supporting Information). Syngnathinae is species rich with highly divergent phenotypes compared with Nerophinae (Hamilton et al., 2017), which might be causally linked to a positive correlation with the rate of neutral molecular evolution. We estimated the ω (dN/dS) value of orthologous protein-coding genes in Syngnathinae and other teleosts and found the highest ω value in the common ancestor of seadragons and two seadragon species (leafy and weedy seadragons) (Figure S3 in Supporting Information).

Genetic signatures for camouflage

Adaptive evolution is one of the most important factors af-

fecting fitness and shaping species distributions (Lohbeck et al., 2012; Walkiewicz et al., 2012). The genetic basis of adaptive traits is expected to be shaped by natural selection (Ge and Guo, 2020; Wei, 2020). This would also be expected for the evolution of the remarkable camouflage and other characteristics of the leafy seadragon. We identified 89 positively selected genes (PSGs), and 269 rapidly evolving genes (REGs) in the leafy seadragon (adjusted $P<0.05$) (Figure S4, Tables S8–S11 in Supporting Information). Among these, genes involved in neurodevelopment, and bone, cartilage and body axis formation stood out and were investigated further (Figure 2A). Leaf-like appendages are a common feature of seadragons, although leafy seadragons have much more ornate and elaborate appendages than other species. The long leaf-like structures are primarily composed of a bone matrix along with connective tissues enriched by collagenous fibers (Qu et al., 2021; Stiller et al., 2015). The identified PSGs and REGs suggest their potential involvement in the formation of leaf-like appendages. For example, genes involved in the BMP (*bmpr1aa*) and NODAL (*ndr1*) signaling pathways, and the HOX (*hoxb1a*) gene families showed signs of positive selection. In addition, alkaline phosphatase (*alpl*), which plays a conserved and important role in vertebrate bone development (Liu et al., 2018), was identified as both a PSG and REG in the leafy seadragon (Figure 2A)—a gene with a central function in osteogenic differentiation and bone mineralization in zebrafish (Ohlebusch et al., 2020).

We specifically retrieved 189 genes related to the development of bone and cartilage and estimated the *dN*/*dS* ratio in leafy and weedy seadragons. Compared with background levels, these genes showed significantly higher *dN*/*dS* ratios in both seadragon species ($P<0.0001$ in leafy seadragon, $P<0.01$ in weedy seadragon), with a slightly (but not significantly) higher rate in the leafy seadragon (Figure 2B).

The leafy seadragon's conspicuous camouflage can even change color to mimic kelp and seagrass, enhancing crypsis further (Groves, 1998). Concordantly, we found evidence of rapid evolution of the KIT proto-oncogene, receptor tyrosine kinase a (*kita*) and oculocutaneous albinism II (*oca2*) in the leafy seadragon (Figure 2A). The encoded proteins regulate chromocyte differentiation and migration, and *kita* knockout zebrafish show abnormal colorless trunks (Santoriello et al., 2010). *Scl2a11*, which contributes to diversification of hues in pigment cells in vertebrates (Kimura et al., 2014), showed positive selection and accelerated evolution in the leafy seadragon (Figure 2A). Together, these results imply that the PSGs and REGs in the leafy seadragon genome might contribute to its remarkable camouflage.

We previously found that the maintenance of leaf-like appendages is largely supported by genes recruited from those involved in the development and maintenance of fins and skin (Qu et al., 2021). Using transcriptomic datasets from leaf-like appendages (on the head, dorsal, and ventral), skin, and fins (Qu et al., 2021), we found that most of the PSGs and REGs had higher expression in the leaf-like appendages than in the fins and skin (Figure 2C). Among these genes, REG bone morphogenetic protein 6 (*bmp6*) was consistently and highly expressed in the leaf-like appendages compared with its expression in other body tissues (Figure 2C). In this study, we generated *bmp6* mutant zebrafish lines using the CRISPR-Cas9 technology. The intermuscular bones (IBs) in $bmp6^{-/-}$ fish were dysplastic and significantly reduced in number compared with those in the wild types, which had no visible phenotypic changes in the axial skeleton, such as the skull, rib, and vertebral column (Figure 2D; Figures S5–S8 in Supporting Information). Consistent results were also reported in Xu's study (Xu et al., 2022). The stable phenotypes of *bmp6* knockout fish further confirmed the crucial function of this gene in the IBs development.

Adaptive changes in nutrient use efficiency and metabolism

Similar to many other syngnathids leafy seadragons inhabit costal seagrass beds, but it differs from their relatives not only in their ornate leaf-like appendages, but also in their larger body size. Fully grown adults can reach a length of 50 cm (Groves, 1998), which may require large amounts of energy for maintenance. Accordingly, we identified several PSGs and REGs that contribute to nutrition and metabolism (Figure 2A). For example, *cyp7a1* encodes a member of cytochrome P450 enzyme and is involved in the synthesis of cholesterol, steroids, and other lipids (Escher et al., 2003; Pullinger et al., 2002). *apoA1*, *cept*, *sort1*, *soat1*, and *abca1* play important roles in cholesterol conversion (Bachmann et al., 2004; Geng et al., 2016; Gustafsen et al., 2014; Oram and Lawn, 2001; Thompson et al., 2008). Moreover, the expanded gene families of the leafy seadragon were enriched in the "glycerolipid metabolism" pathway (Figure 2A; Tables S12 and S13 in Supporting Information). Animals with larger body sizes usually require higher energy metabolism, and these genetic changes in the leafy seadragon may improve its nutrient use efficiency, thus allowing for a larger size at maturity.

Simultaneous evolution of vision and olfaction

Leafy seadragons have a sufficiently well-developed vision to not only detect small prey organisms but also to visually assess their surroundings for camouflage (Telgársky, 2014). We found that numerous genes involved in the structure of the eyes significantly diverged between the leafy seadragon and other teleosts (Figure 2A). The PSGs and REGs *ascl1a*, and *gnl3* are necessary for retinal development (Campbell and Okamoto, 2013; Endo et al., 2009), while *fzd8a* and *opa1*

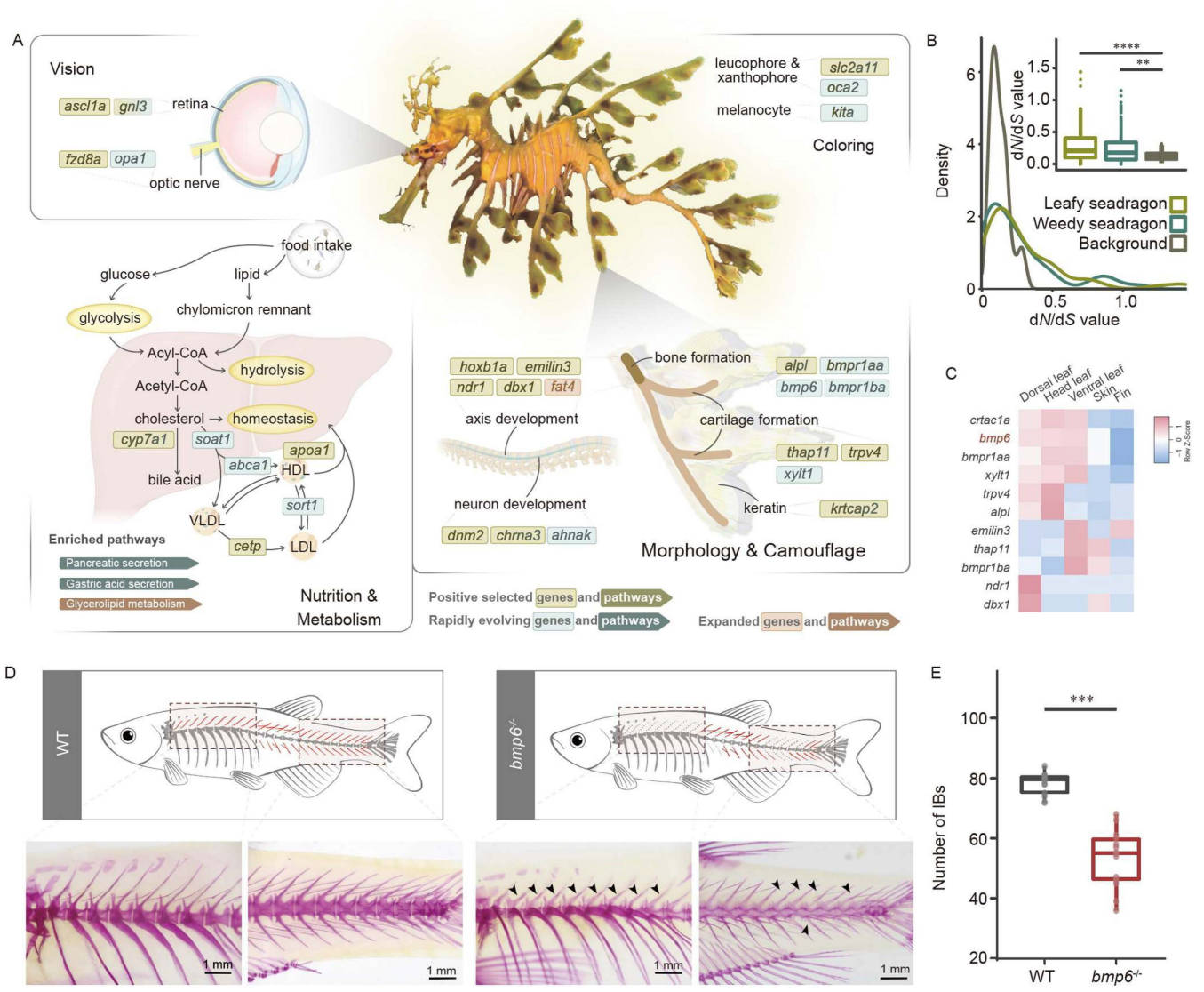

Figure 2 Genomic features related to the particular leafy seadragon biology. A, PSGs, REGs, expanded genes and pathways in the leafy seadragon genome are associated with vision, coloration, nutrition & metabolism, and morphology & camouflage. B, A total of 189 genes in Gene Ontology (GO) terms related to the development of bone and cartilage were selected, and we calculated the *dN*/*dS* ratios in the leafy seadragon and weedy seadragon under the two-ratio branch model (model 2) of PAML. Background *dN*/*dS* ratios were calculated under one-ratio branch model (model 1) of PAML. The distribution densities of the *dN*/*dS* values are shown. A box plot of *dN*/*dS* values in different body size categories is shown. The mean *dN*/*dS* values in leafy seadragon and weedy seadragon were both significantly larger than the background value. ****, $P<0.0001$; **, $P<0.01$. C, Expression pattern of genes related to bone and cartilage formations in the leaf-like appendages, skin, and fin in the weedy seadragon. D and E, Phenotypes and statistics of *bmp6* knockout mutants showing that IBs are dysplastic and significantly reduced in number in zebrafish (*** $P<0.001$). The bone was stained with Alizarin red. The black arrowheads indicate that the IBs disappeared in the mutant.

are core genes for the optic nerves (Savvaki et al., 2021; Yarosh et al., 2008). Among them, knockout of *gln3* led to the absence of retinal cone and optic tectum apoptotic cells (Paridaen et al., 2011), and that of *fzd8a* resulted in optic fissures in zebrafish (Cheng et al., 2018).

Previous studies in both mammals and fish hypothesized that enhanced vision comes with an evolutionary consequence of receded olfaction, which suggests a trade-off in sensory acuity (Nummela et al., 2013; Wang et al., 2022). In the present study, we found that the sense of smell may have been secondarily reduced in the two seadragon species (Figure 3A; Tables S14–S17 in Supporting Information). Generally, vertebrates have five types of evolutionarily distinct multi-gene families of G-protein-coupled receptors (GPCRs) to detect chemicals in the environment: odorant receptors (ORs), trace-amine associated receptors (TAARs), vomeronasal type 1 and type 2 receptors (V1R and V2R), and the mammal-specific formylpeptide receptors (FPRs) (Manzini and Korsching, 2011; Mombaerts, 2004). In teleosts, homologs of V1Rs and V2Rs are also named ORAs (ORs related to class A GPCRs) and OlfCs (ORs related to class C GPCRs) because of their independent monophyletic entities and lack of vomeronasal organ in fish (Hussain, 2011). A previous study on seahorses revealed a significantly smaller

repertoire of ORs (26 genes) than is typical for teleosts (33–160 genes) (Lin et al., 2016). By retrieving the complete OR, TAAR, ORA/V1R, and OlfC/V2R gene repertories in eight syngnathids and nine other teleost fishes, we found that OR contraction is the ancestral feature of syngnathids (<35 genes in all species). Seadragons exhibited an even greater loss of olfaction-related genes (9 and 10 genes in leafy and weedy seadragons, respectively) and possess the, so far, smallest repertoire of any ray-finned fish genome (Figure 3A; Figures S9–S12, Tables S18 and S19 in Supporting Information). Notably, in addition to the contraction in ORs, significant gene loss of TAARs and OlfCs/V2Rs was also found in the common ancestor of syngnathids (Figure 3A; Figures S13–S19 and Tables S20–S23 in Supporting Information), implying weakened olfaction in these taxa.

In contrast to other olfactory receptor families characterized by very dynamic evolutionary gains and losses of functional genes, the ORA/V1R family—which consists of the same six genes—is strikingly conserved in teleost species (Zapilko and Korsching, 2016). Interestingly, seadragons retained only two (*ora2* and *ora5*) of these six genes, whereas seahorses, pipefishes, and other teleosts typically have five to six (Figure 3A; Figure S15, Tables S24 and S25 in Supporting Information). ORAs respond to pheromonal signals, thereby playing vital roles in mating preferences, aggression control, individual recognition, and migration. In zebrafish, ORAs can detect phydroxyphenylacetic acid and bile acids/salts (Ahuja and Korsching, 2014; Cong et al., 2019). The extreme loss of ORAs/V1Rs coincides with the solitary behavior in seadragons, suggesting that they depend less on their sense of smell and taste to navigate through the seagrass.

Unlike ORAs/V1Rs, OlfCs/V2Rs detect amino acids (AAs) and elicit feeding behavior in fish (Luu et al., 2004). For example, in cichlids, the large OlfC/V2R repertoire is suspected to contribute to their extraordinary feeding behavior diversification (Nikaido et al., 2013). In seadragons, besides the reduced gene copy, there are fewer conserved AA sequences. Some seadragon-specific changes were detected in the AA-sensing ligand-binding receptor signature motif (Figure 3D and E). As it remains unclear whether these changes have any effects on the binding ability or preference of these receptors in seadragons, further studies are needed to clarify their functional consequences.

Historic population dynamics

Originating in temperate Australasia, Syngnathinae underwent rapid episodes of diversification after splitting from Nerophinae (Santaquiteria et al., 2021; Stiller et al., 2022). Currently, they are widely distributed in tropical and warm-temperate regions, with extant diversity occurring across the Indo-Pacific (Figure S20 in Supporting Information). However, species living in temperate Australasia have been largely restricted to this region (Stiller et al., 2022) (Figure 4A; Table S26 in Supporting Information)—including two highly endemic seadragon species in the coastal waters of southern Australia.

For teleosts, speciation and habitat colonization rates and population size were greatly affected by drastic climate change and shifting ocean currents in the Neogene and Quaternary (Li et al., 2021b). To infer the demographic histories of syngnathids, we used whole-genome datasets to investigate the changes in the effective population size (*Ne*) in eight species with different distributions (Figure 4B) using both the pairwise sequentially Markovian coalescent (PSMC) and multiple sequentially Markovian coalescent (MSMC) methods (Li and Durbin, 2011; Schiffels and Durbin, 2014). The trends revealed with these methods were consistent in most cases (Figure 4C; Figure S21 in Supporting Information).

We also found that the population histories of syngnathids distributed in southern Australasia and the west Atlantic regions are related to eustatic sea-level fluctuations, as demonstrated by the evident drastic decline in *Ne* ~100 thousand years ago (kya), which coincided with the inception of the Last Glacial Period (LGP, approximate 110–12 kya) (Figure 4C). However, the *Ne* of the southern Australasian species has remained low until today, despite global temperatures and sea levels having risen again and the *Ne* of other syngnathids increasing. These Australasian species, in particular the leafy and the weedy seadragons (Figure 4C), have also had relatively smaller *Ne*s than those in other regions. Moreover, population studies on the leafy seadragon have estimated a particularly low genetic diversity (Stiller et al., 2021; Stiller et al., 2016), which corresponds to a relatively gradual and much smaller change in *Ne* than in any other syngnathid species.

Habitat suitability under climate change

Using the maximum entropy approach, we then explored the distribution of each syngnathid species during the present and Last Glacial Maximum (LGM, ~21 kya) (Figure 5; Table S27 in Supporting Information). Manado pipefish were excluded from this analysis because they live in both brackish and freshwater (Froese and Pauly, 2022), for which the models are largely different from those of marine species and thus have low comparability. The predicted distribution range was consistent with the extant distribution of all seven species (Figure 4B; Figure S22 in Supporting Information). Habitat suitability was largely reduced for most species during the LGM, which might to some extent explain the drastic decline in *Ne* (Figures S23 and S24 in Supporting Information).

We additionally estimated possible changes in the suitable

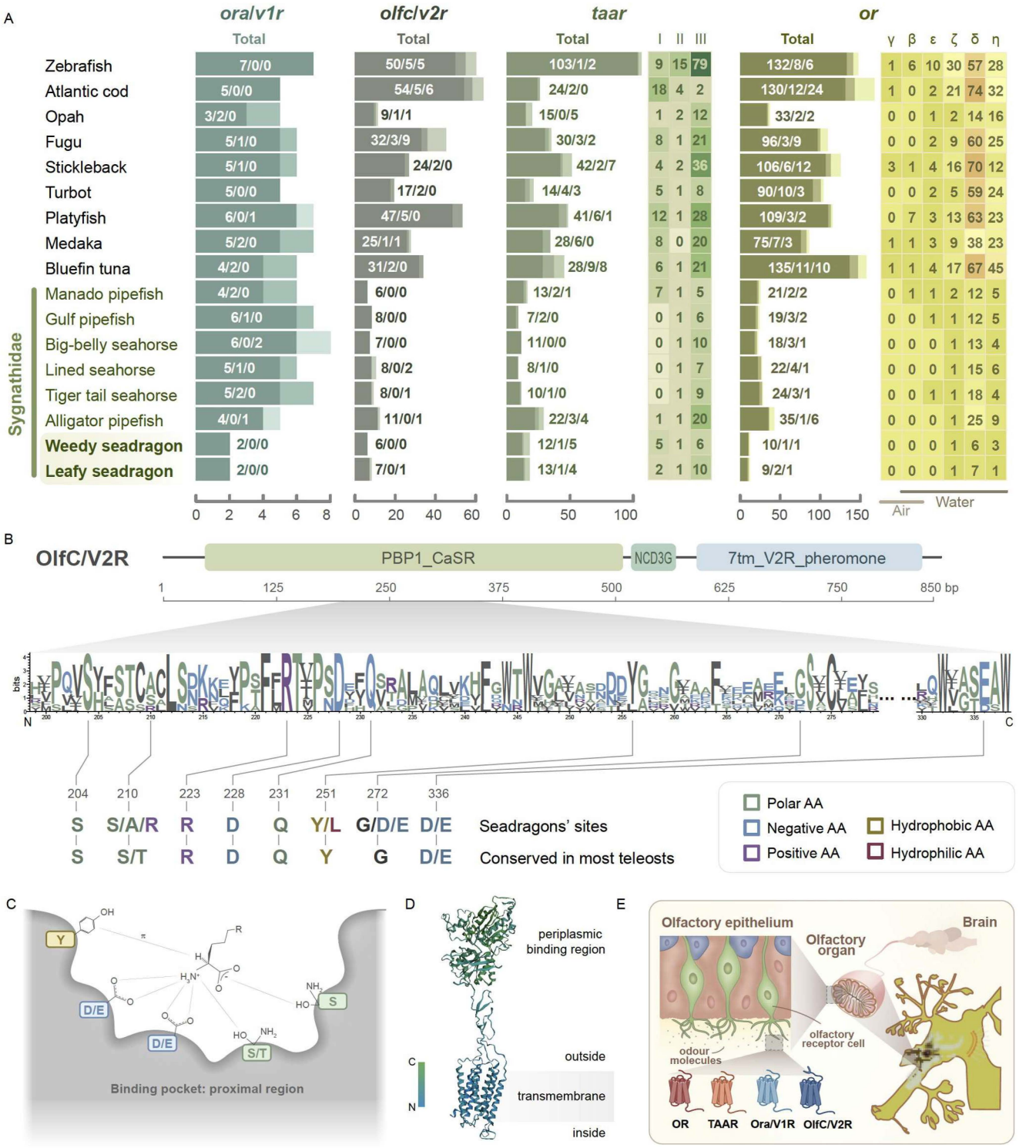

Figure 3 Evolutionary characteristics of four olfactory receptor families in eight syngnathid species and other representative teleosts. A, Number of genes belonging to each olfactory receptor family and subfamily. The dark, intermediate, and light bars represent functional genes, truncated genes, and pseudogenes, respectively. The numbers in each bar indicate those of functional genes, truncated genes, and pseudogenes, respectively. For TAAR, three subfamilies were identified as class I, II and III, respectively, whereas for OR, six subfamilies (γ, β, ε, ζ, δ, and η) are identified. The numbers of functional genes for each subfamily are shown in boxes. "Air" and "Water" represent the detection of airborne and water-soluble odorants, respectively. B, AA-sensing ligand-binding receptor signature motif (updated from Silva and Antunes, 2017). C, Probable AA interactions are represented in the binding pocket. Sequence logo based on leafy Seadragon OlfC/V2R gene alignment. D, Structure of leafy seadragon OlfC/V2R predicted using I-TASSER (C-score=−0.13, TM-score=0.70±0.12), showing the seven transmembrane domains and periplasmic binding region. E, General characteristics of the fish olfactory system, with the four olfactory receptor families expressed in the olfactory epithelium.

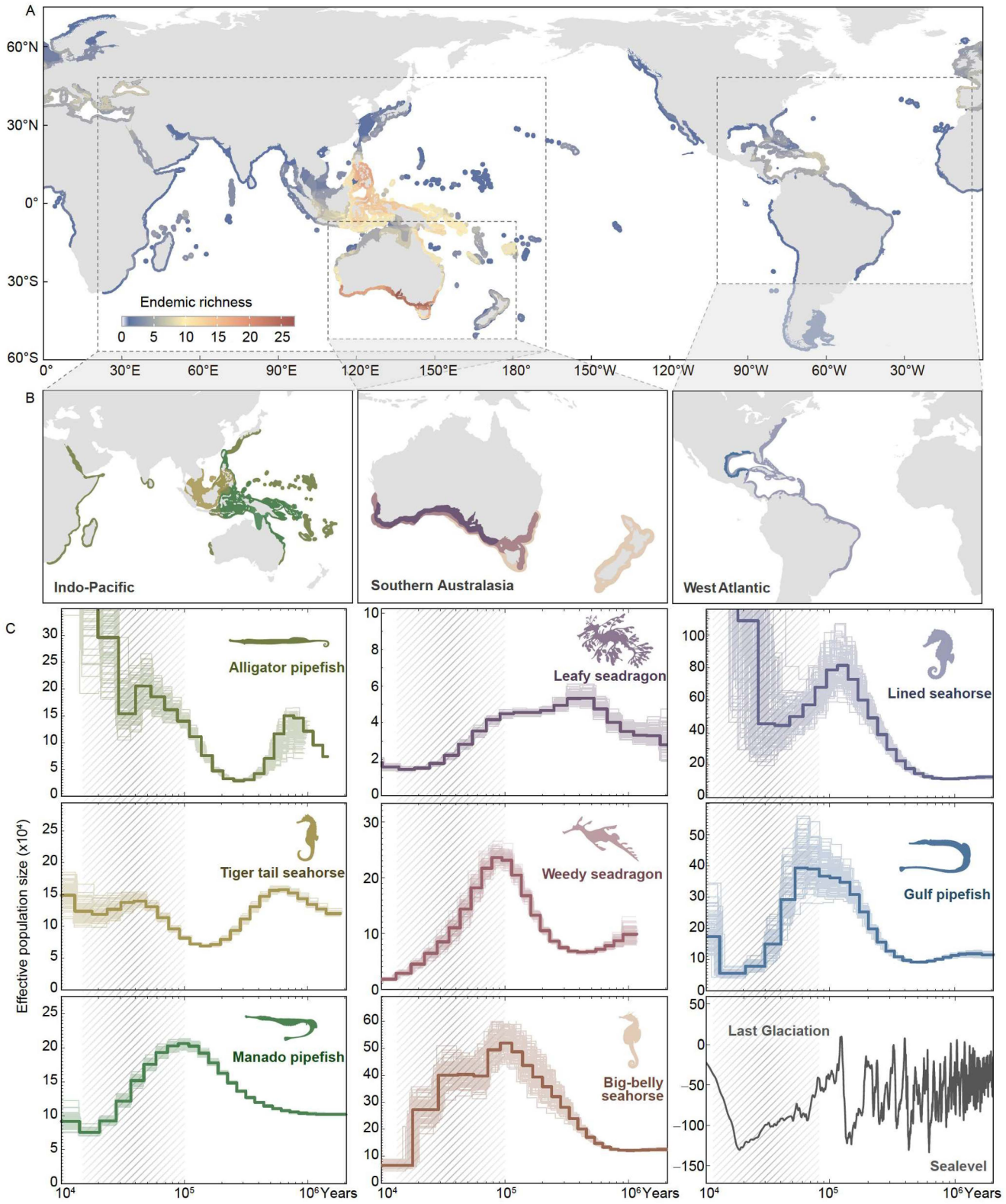

Figure 4 Endemic richness, distributions, and demographic trajectories of syngnathid species. A, Spatial distributions of endemic richness in Syngnathidae based on range maps from IUCN. B, Current distribution ranges of eight syngnathid species. Indo-Pacific region: Alligator pipefish, olive; Tiger tail seahorse, yellow; Manado pipefish, green; Southern Australasia: Leafy seadragon, purple; Weedy seadragon, red; Big-belly seahorse, khaki; West Atlantic: Lined seahorse, violet; Gulf pipefish, blue. C, Demographic trajectory of eight syngnathid species obtained using the PSMC method. The *x*-axis corresponds to time before present in years on a log scale, while the *y*-axis corresponds to the effective population size (*Ne*). The lower right-hand plot shows the sea level (m) with the same *x*-axis as before. The shadow indicates the Last Glaciation.

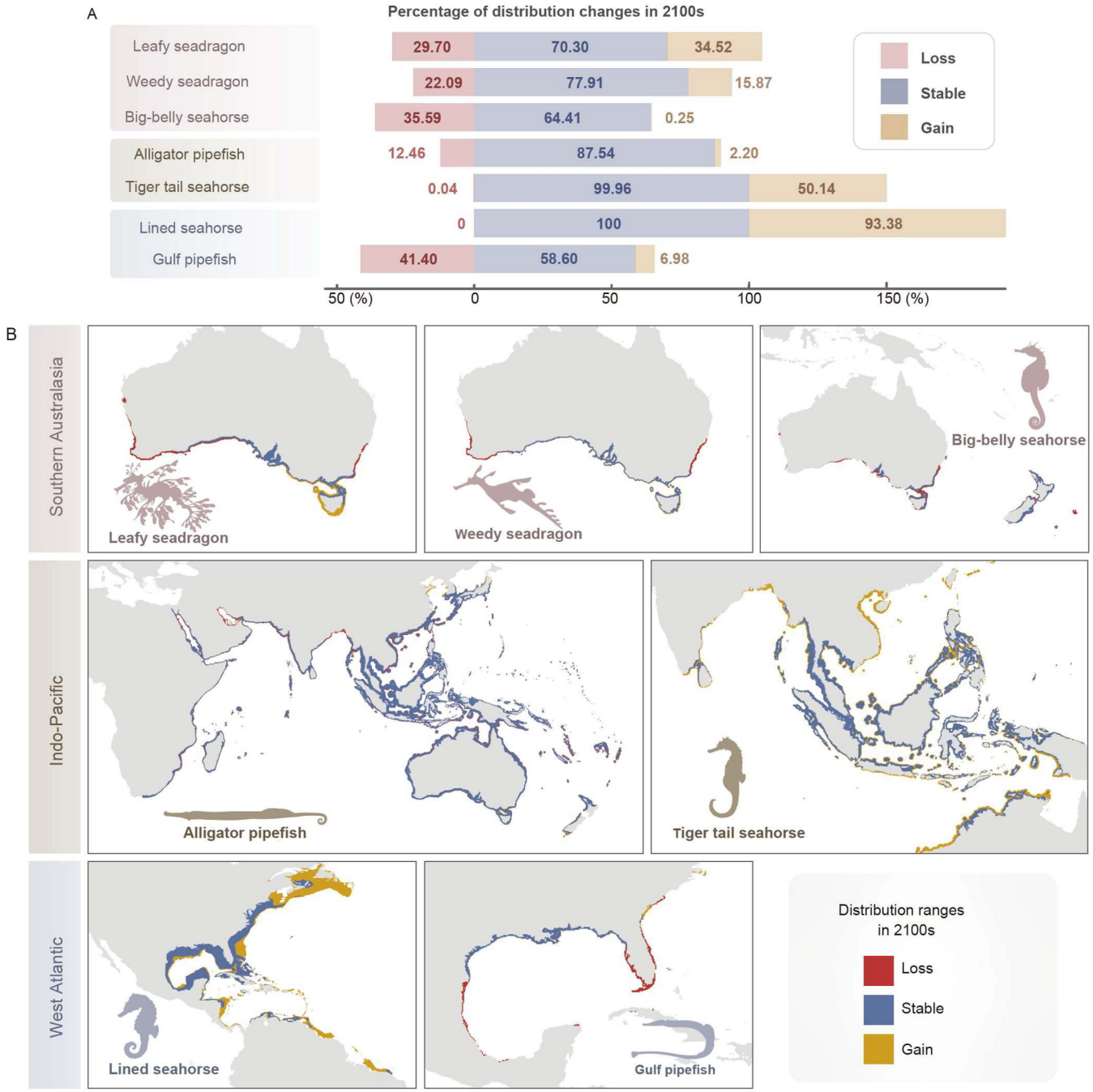

Figure 5 Habitat suitability changes for seven syngnathid species projected by maximum entropy models under the RCP 8.5 scenario in the 2100s. A, Percentage of distribution changes. Names in the three boxes from top to bottom indicate species distribution in southern Australia, Indo-Pacific, and West Atlantic regions, respectively. B, Changes in binary habitat suitability for each species. The category "stable" represents areas predicted to be suitable under both present-day and future climatic conditions, "loss" indicates areas predicted to be suitable under present-day conditions but unsuitable in the future, and "gain" indicates areas predicted to be unsuitable under present-day conditions but suitable in the future.

habitats of syngnathid species under representative concentration pathway (RCP) 8.5 in 2090–2100. The SDMs predicted considerable future loss (22% to 41%) of suitable areas for three southern Australasian species and the Gulf pipefish endemic to the Gulf of Mexico (Figure 5; Table S28 in Supporting Information). Research on terrestrial plants and animals has shown that endemic species usually have narrower niches, making them more sensitive to global environmental changes (Sala et al., 2000). A similar situation was also observed for syngnathids. Compared with the widespread lined seahorse and alligator pipefish, endemic seadragons can only tolerate a limited range of environmental gradients and thus have much narrower realized niches (Figure S25 in Supporting Information).

For the two seadragon species, the lost suitable areas in 2090–2100 were mainly on the east and west coasts of

Australia (Figure 5B). The leafy seadragon populations in Western and South Australia are demographically independent units (Stiller et al., 2021; Stiller et al., 2016), and similar results were also reported for the weedy seadragon (Wilson et al., 2017). Despite declining population sizes, low genetic diversity, loss of habitat, and limited gene flow between populations potentially making seadragons more vulnerable to further global changes, the SDMs demonstrated potential gain of habitat areas for the leafy seadragon (35%), the tiger tail seahorse (50%), and particularly, the lined seahorse (93%) (Figure 5B). However, syngnathids have low-dispersal life histories (Browne et al., 2008), indicating that they may not be able to efficiently emigrate to suitable habitats that form in the future.

DISCUSSION

With the development of the sequencing technology, genome-wide analysis became an effective way to reveal animal traits evolution (Ahlberg, 2021; Chen and Huang, 2020). In this study, we produced a *de novo* assembled genome of the leafy seadragon and identified signatures of rapid evolution and positive selection in genes related to the formation of camouflage color and appendages. Accelerated evolutionary rate and rapid natural selection are usually key factors for adaptive radiation and hence, diversification of morphology and behavior (Lü et al., 2021; Weber et al., 2020). The neutral evolutionary rate in the leafy seadragon was higher than that in other teleosts in the ancestral branch of the subfamily Syngnathinae, which might explain their rapid and drastic phenotypic diversification, including the evolution of their defining skin appendages (Shepherd et al., 2017). Furthermore, rapid evolution and positive selection have been shown to correlate with specific morphological and physiological traits in many fish lineages, including jaw and tooth phenotypes in cichlids (Karagic et al., 2020), body plan asymmetry in flatfishes (Lü et al., 2021), and the extreme lifespan of rockfishes (Kolora et al., 2021). Seadragons were reported to loss some key *fgf* genes, which were involved in the morphogenesis of traits (Small et al., 2022; Xiao et al., 2020). In the present study, we further identified genetic signatures in the leafy seadragon that may have contributed to its extraordinary camouflage and keen eyesight (Branshaw, 2005). Syngnathids often exhibit a reduced olfaction-related gene repertoire, suggesting an evolutionary trade-off with the visual system that seems to have increased in genetic complexity and possibly acuity. Gradual gene loss events have been observed in chemosensory receptors of syngnathids, with seadragons retaining the smallest repertoire. Previous studies have documented associations between changes in chemosensory receptor repertoires and ecological niches. For example, the expansion of OR genes in freshwater fish may allow them to detect a wider range of odorant stimuli that are important for their survival in freshwater (Liu et al., 2021), whereas the small numbers of ORs and TAARs in Mariana snailfish may be related to the low abundance and diversity of organisms and biomass in the hadal trenches (Jiang et al., 2019). The SDMs in this study predicted significantly smaller realized niches for seadragons than for their widespread relatives. Hence, we suspect that the simplified but specific olfactory receptors in seadragons are related to ecological adaptation to the highly specialized, environments of kelp forests and seagrass beds.

Leafy seadragons evolved to camouflage within their habitat. However, this highly specialized ecological niche and habitat also led to a high dependency on its specific habitat type, and thus climate change-related habitat loss is a major threat to leafy seadragon populations. The SDM predictions indicated that the leafy seadragon had experienced a dramatic range shift over the course of this century. The limited dispersal capacity and specific habitat requirements of these fish are likely to amplify their vulnerability to environmental change and reduce the efficiency of protected areas and prospective suitable habitats that are geographically distant from their current habitat. Therefore, assessment of the vulnerability of the leafy seadragon and an informed conservation plan needs to consider more than just the species population dynamics; the everchanging habitat in the face of global climate change must also be considered. For example, a long-term empirical study from the 2000s demonstrated that kelp forests in a tropical-temperate transition zone in eastern Australia are subjected to considerable warming due to climate change and have become increasingly dominated by tropical herbivores. This consequently resulted in the gradual decline and disappearance of the kelp (Vergés et al., 2016). Hence, the conservation and management of the leafy seadragon need to also consider the protection of seagrass and kelp habitats. Specifically, we recommend taking climate change-induced range shifts into account while developing future protection strategies.

MATERIALS AND METHODS

Sampling

A small tissue clip was collected from a tail leaf-like appendage that naturally fell from an adult leafy seadragon (*Phycodurus eques*) provided by LanHai Co., a transport company responsible for transporting live animals to aquariums in Guangzhou, without harming the animal. The tissues were then stored in 95% ethanol.

DNA extraction and sequencing

Genomic DNA was extracted from the tissue clip using the

classic phenol-chloroform method, followed by purification with the QIAGEN Genomic kit (Qiagen, USA) according to the standard operating procedure provided by the manufacturer. For sequencing, a total of 30.14 Gb of PacBio reads and 34.55 Gb of Illumina reads were sequenced using a PacBio Sequel II platform and an Illumina HiSeq 2500 instrument, respectively. Raw sequencing data were processed following the quality control protocol using SMRTlink 8.0 to remove low-quality reads and adapters, resulting in subreads.

Genome assembly

k-mer analysis was performed prior to genome assembly to estimate the genome size and heterozygosity (Gnerre et al., 2011). Quality-filtered reads were subjected to *17*-mer frequency distribution analysis. By analyzing the *17*-mer depth distribution from the shotgun-cleaned sequencing reads, we estimated the genome size of the leafy seadragon as follows: genome size=K_{num}/K_{depth}.

The genome was assembled *de novo* into contigs based on PacBio long reads using FALCON (Li et al., 2012), string graph (Myers, 2005), and hifiasm (Cheng et al., 2021) with optimized parameters. The assembly was then polished with BLASR (Chaisson and Tesler, 2012) by mapping PacBio reads back to the contigs. To further improve the accuracy of the assembly, the contigs were refined with Nextpolish using Illumina short reads with the default parameters (Hu et al., 2020). To discard possibly redundant contigs and generate a final assembly, similarity searches were performed using Redundans software with the parameters "identity 0.8 –overlap 0.8".

The completeness of genome assembly was assessed using BUSCO v4.0.5 (Benchmarking Universal Single-Copy Orthologs) with the actinopterygii_odb10 database (3,640 single-copy genes) (Simão et al., 2015).

Genome annotation

We identified repeats and TEs using *de novo* approaches. GMATA (Wang and Wang, 2016) and TRF (Benson, 1999) were used to identify tandem repeats under default parameters. LTR_FINDER (Xu and Wang, 2007) was used to identify long terminal repeat retrotransposons, and the "einverted" tool in EMBOSS (https://www.bioinformatics.nl/cgi-bin/emboss) was used to detect the terminal inverted repeats. RepeatMasker (Tarailo-Graovac and Chen, 2009) and RepeatProteinMask v3.3.0 (http://www repeatmasker.org/) were employed to identify TEs based on homology searches against the Repbase library v16.03, (https://www.girinst.org/repbase/) using the parameters "-nolow -no_is -norna -parallel 1" and "-noLowSimple –pvalue 1e-4". An *ab initio* TE library was constructed by integrating two repeat finding programs, RECON and RepeatModeler v1.08 (http://www.repeatmasker.org/RepeatModeler.html). Using the repeat library, we estimated the repeat content of the leafy seadragon genome using RepeatMasker with the sensitive mode (-s) option.

Ab initio gene prediction was performed using three programs, namely Augustus (Stanke and Waack, 2003), GlimmerHMM (Majoros et al., 2004), and SNAP (Korf, 2004). The GeMoMa program (Keilwagen et al., 2016) was run for homology-based prediction by aligning the assembled genome against zebrafish (*Danio rerio*), Japanese medaka (*Oryzias latipes*), lined seahorse (*Hippocampus erectus*), tiger tail seahorse (*H. comes*), and weedy seadragon (*Phyllopteryx taeniolatus*). Next, the transcriptome data of weedy seadragon from our previous study (Qu et al., 2021) was mapped onto the genome, and gene prediction was performed using TransDecoder (http://transdecoder.github.io) and GeneMarkS-T (Tang et al., 2015). PASA (Campbell et al., 2006) was used to predict unigene sequences without reference assembly, based on transcriptome data. We then combined the results from these three methods with EvidenceModeler (Haas et al., 2008). The functions of the predicted genes were annotated using InterProScan v 5.15 (Jones et al., 2014) against public protein databases. In addition, the KEGG (Kanehisa and Goto, 2000), NR (Birney et al., 2004), SwissProt (Release 2011.6), and TrEMBL (Release 2011.6) databases were searched for homology-based functional assignments using BLAST software v2.6.0.

Syntenic analysis

We performed a genome-wide syntenic analysis between the leafy seadragon and weedy seadragon. BLASTP was used to identify orthologous genes in the pairs of these species. Synteny blocks were searched for seeds with at least five consecutive orthologous genes between each pair of species. Subsequently, the proportion of synteny between the pairs of species was calculated. A circos plot of the leafy seadragon-weedy seadragon was generated (Figure S1 in Supporting Information).

Phylogenomic analysis

To determine the phylogenetic position of the leafy seadragon with respect to other Syngnathidae fish, we performed phylogenomic analysis using whole-genome protein datasets from several representative ray-finned fish. Protein datasets were obtained from Ensembl-FTP release-96 (fugu, *Takifugu rubripes*; stickleback, *Gasterosteatus aculeatus*; medaka, *O. latipes*; Nile tilapia, *Oreochromis niloticus*; turbot, *Scophthalmus maximus*; greater amberjack, *Seriola dumerili*; giant fin mudskipper, *Periophthalmus magnuspinnatus*; zebrafish, *D. rerio* and spotted gar, *Lepisosteus oculatus*) or other sources—Southern bluefin tuna, *Thunnus*

orientalis (Suda et al., 2019); Atlantic cod, *Gadus morhua* (gadMor2) (Tørresen et al., 2017); Asian arowana, *Scleropages formosus* (Bian et al., 2016); Pacific opah, *Lampris incognitus* (Wang et al., 2022); tiger tail seahorse, *H. comes* (Lin et al., 2016); lined seahorse, *H. erectus* (Li et al., 2021a); Big-belly seahorse, *H. abdominails* (He et al., 2021); Gulf pipefish, *Syngnathus scovelli* (Small et al., 2016); alligator pipefish, *Syngnathoides biaculeatus*; weedy seadragon, *P. taeniolatus* (Qu et al., 2021); Manado pipefish, *Microphis manadensis* (Zhang et al., 2020) and leafy seadragon, *P. eques* (present study). OrthoFinder v 2.2.7 (Emms and Kelly, 2015) with default settings was used to identify one-to-one orthologs from the 21 ray-finned fish species. Multiple alignments were generated for each orthologous group using MAFFT v7.475 (https://mafft.cbrc.jp/alignment/software/). gBlocks was used to remove poorly aligned regions for each of the orthologous groups with the "allowed gap positions" set to "With Half". After alignment and trimming, all the one-to-one orthologous genes were concatenated into a single supergene. ProteinModelSelection.pl provided with RAxML v8.2.12 (Stamatakis, 2014) was used to deduce the best-suited substitution model for concatenated alignment. A maximum likelihood (ML) tree was generated using RAxML. For the ML analysis, we used the best-fit substitution model, as deduced by ProteinModelSelection.pl, and 1,000 replicates for bootstrap support (Figure S2 in Supporting Information). Molecular dating was performed using MCMCtree v4.9j in the PAML software v4.9h. The time calibration was based on a total of eight calibration points, including three dated fossil records: (i) †*Acentrophorus varians* (~254–260 Ma ago), the oldest known neopterygian; (ii) †*Plectocretacicus clarae* (~97–153 Ma ago), earliest stem tetraodontiform; and (iii) †*Prosolenostomus lessenii* (~48–50 Ma ago), the oldest syngnathid fossil (Stiller et al., 2022; Teske and Beheregaray, 2009).

Population historical dynamics

The demographic history of the leafy seadragon and the other seven syngnathid species was inferred using both the PSMC (Li and Durbin, 2011) and MSMC methods (Schiffels and Durbin, 2014). For each species, Illumina reads were aligned to the genome using BWA to recover diploid genome heterozygosity information. Variable sites were identified using SAMtools (Li and Durbin, 2009). The whole-genome diploid consensus sequences were generated using SAMtools and BCFtools (Li, 2011) based on the parameter with C50 -d8000 -uf. The program fq2psmcfa was used to transform the consensus sequence into a FASTA-like format, where the characters indicate heterozygous positions in consecutive bins of 100 bp. The PSMC analysis consisted of the following parameters: N25–t15–r5–p "4+25*2+4+6". In addition, 100 bootstrap replicates were obtained to measure the uncertainty around the parameter estimates. MSMC started from a bam-file created by SAMtools and generated a mask-file using BEDtools genomecov (Quinlan and Hall, 2010). We then separated the chromosomes and generated input files using generate_multihetsep.py in msmc-tools. The MSMC program was run with parameters t27. The mutation rate for each species was estimated based on the phylogenetic tree and divergence time. Changes in the effective population size (*Ne*) of each species were calculated using a mutation rate (μ) of 4.33×10^{-9} per site per year and a generation time (g) of one year (Li et al., 2021a; Lin et al., 2016).

Ecological niche analyses

Study area and distribution data

Distribution data of the leafy seadragon and six other syngnathid species were collected from the published literature and various online repositories, including the Global Biodiversity Information Facility (http://www.gbif.org), Ocean Biogeographic Information System (http://iobis.org), USGS Biodiversity Information Serving Our Nation (https://bison.usgs.gov), and Atlas of Living Australia (http://www.ala.org.au). The retrieved records were checked by experts on syngnathid and invalid records such as outside species natural distributional range were excluded. To correct for sampling bias, we filtered the presence records by keeping one record per 5-arcmin grid cell (Hu et al., 2021; Kramer-Schadt et al., 2013). Ultimately, 111–1,211 records were retained for each species (Figure S22 in Supporting Information).

Predictor variables

We used predictors from MARSPEC (Sbrocco and Barber, 2013) and Bio-ORACLE (Assis et al., 2018) to project habitat suitability for syngnathids in paleo-and future climates, respectively. We checked collinearity among the predictors and selected one among the highly correlated predictors (Hu et al., 2021). We ultimately considered six (water depth, distance to shore, annual mean sea surface salinity (SSS), annual range of SSS, annual mean sea surface temperature (SST), and annual range of SST) and seven (plus annual mean current velocity) predictors to project habitat suitability during the Last Glacial Maximum and the average of 2090–2100, respectively (Figure S23 in Supporting Information). We obtained projections of marine predictors in the 2100s under the RCP 8.5, and the importance of each predictor was quantified (Figure S26 in Supporting Information).

Realized niche quantification

We quantified the realized niches for the leafy seadragon and its relatives using Hutchinson's *n*-dimensional hypervolume approach. We first extracted marine predictors from the

presence records for each species and scaled them to zero means and unit variance. We then used the *hypervolume* R package to determine the shapes and volumes of the realized niches for each species (Blonder et al., 2018).

Species distribution model

We constructed SDMs using the MaxEnt algorithm, which is a machine learning approach that has been widely used in the marine realm (Melo-Merino et al., 2020). In principle, we developed SDMs based on species present-day distribution data and present-day marine predictors and then applied this model to project species habitat suitability during different time periods. Therefore, we developed two SDMs for each species: one model to project habitat suitability during the LGM, and the other to investigate possible future changes in habitat suitability. To avoid overfitting issues associated with model default parameter settings, we tuned MaxEnt parameters using the *ENMeval* R package (Kass et al., 2021). Predictive abilities of SDMs were evaluated using the area under the receiver operating characteristic curve (AUC) and continuous Boyce index. For easy interpretation, we converted continuous SDM predictions into binary through 10% presence probability threshold. For each species, we calculated the ratio of the suitable habitat area during the LGM to the present-day suitable habitat area. When projecting future habitat suitability, we adopted an unlimited dispersal scenario that assumes that species can occupy any new suitable habitat in the future. In addition, the coefficient of variation (i.e., the standard deviation divided by the mean), which measures model agreement levels (a lower value indicates higher agreement), was estimated. Generally, the coefficient of variation values was low, especially within the projected suitable areas (Figures S27 and S28 in Supporting Information), suggesting that our model predictions should be reliable.

Expansion and contraction of gene families

We compared the protein sequences of leafy seadragon with that of 12 other ray-finned fish, including zebrafish, opah, medaka, fugu, Southern bluefin tuna, tiger tail seahorse, lined seahorse, big-belly seahorse, Gulf pipefish, weedy seadragon, alligator pipefish, and Manado pipefish, for identifying potential homologs using BLASTP with an *E*-value of 1×10^{-10}. OrthoFinder version 2.5.2 was used to identify orthogroups with the default MCL inflation parameter (Emms and Kelly, 2015). First, OrthoFinder uses DIAMOND for sequence similarity searches in all-versus-all mode. The OrthoFinder algorithm was then used to initially process the DIAMOND search results, connect putative homologues, and determine the final scores for each species to the graph file. The Markov cluster algorithm (MCL) was used to cluster gene families. The numbers and sequences of the orthogroups are written into files. Expansion and contraction in the gene family were calculated using the CAFÉ program v3.1 (De Bie et al., 2006) with the gene family counts file and species tree as input based on the birth-and-death model. The parameters "-p 0.01, -r 10000, -s" were set to search for the birth and death parameter (λ) of genes based on Monte Carlo resampling, and birth and death parameters in gene families with a P value≤0.01 have been reported. Gene families without homology in the SWISS-PROT database were filtered out to reduce potential false-positive expansions or contractions caused by gene prediction. Gene families containing sequences with multiple functional annotations were then removed. Gene expansion and contraction results for each branch of the phylogenetic tree were estimated and are summarized in Figure S4 in Supporting Information. In addition, GO and KEGG enrichment analyses of expanded and contracted gene families in the leafy seadragon and leafy-weedy seadragon clades were conducted using the GOseq R package and KOBAS software, and the results are shown in Figures S9, S10, Tables S12–S17, S29 and S30 in Supporting Information.

Positive selection analysis

PSGs in the leafy seadragon and the leafy-weedy seadragon clade were detected. Orthologous genes were extracted from the same species as in the gene family analysis. Coding sequence alignments were generated using the PRANK v. 170427 software with the codon model (Löytynoja, 2014). Positive selection analyses were conducted using the branch-site model with the PAML (Yang, 2007). We compared model A (allows sites to be under positive selection; fix_omega=0) with null model A1 (sites may evolve neutrally or under purifying selection; fix_omega=1 and omega=1) via a likelihood ratio test using the Codeml program in PAML. The significance (adjusted P<0.05) of the compared likelihood ratios was evaluated using χ^2 tests from PAML. Next, GO and KEGG enrichment analyses were performed for PSGs (Tables S8–S11 and S31–S37 in Supporting Information).

Rapid evolution analysis

REGs were detected in the leafy seadragon and the seadragon clade were detected, respectively. Orthologous genes were extracted from the same species as in the gene family analysis. The branch model in PAML was used with the null model (model=0), which assumed that all branches had evolved at the same rate, and the alternative model (model=2). A likelihood ratio test was conducted to examine whether the foreground branch exhibited a significantly higher ω value (regardless of whether it was greater than 1) than the background branch. Genes with adjusted P<0.05

were considered to evolve at a significantly faster rate in leafy seadragon. GO and KEGG enrichment analyses were performed for the REGs (Tables S8–S11 and S31–S37 in Supporting Information).

CRISPR-Cas9-based knockout of *bmp6*

CRISPR/Cas9 strategy was used to generate a *bmp6* mutant zebrafish line. Zebrafish were kept at 26–28°C under a controlled light cycle (14 h light, 10 h dark) to induce spawning. Offspring were used for subsequent experiments. The guide RNAs (gRNAs) were designed to target zebrafish *bmp6* in exon 5 (Figure S5 in Supporting Information) according to the study by Moreno-Mateos et al. (2015). The gRNA template DNA for the *in vitro* transcription was made using the following overlap PCR system, before being run at 98°C for 30 s, 45 cycles of (98°C for 10 s, 60°C for 10 s, 72°C for 15 s), 72°C for 5 min, 10°C for storage.

The generated gRNA template and synthesized Cas9 plasmid (pCS2-nCas9n) DNA were then used for *in vitro* transcription using the mMachine T7 Transcription Kit (Thermo Fischer Scientific, USA), and purified using the RNA cleanup protocol from the RNAeasy mini kit (Qiagen, Germany). Purified gRNAs (~80 ng μL^{-1}) were co-injected with Cas9 mRNA (~400 ng μL^{-1}) into zebrafish embryos (F0 fish) at the single-cell stage. F0 fish were raised to maturity and genotyped using fin clipping. The corresponding primers (forward: bmp6_F:5′ GGTGTAGTATAATGCAATAC 3′; reverse: bmp6_R:5′ CCACTGCTGGTCTCCACACTGA 3′) were used to screen founders with site mutations. Adult founders were outcrossed with wild-type fish to obtain F1 fish, which were subsequently genotyped and outcrossed with wild-type fish to obtain F2 fish. Heterozygous F2 individuals were intercrossed to obtain homozygous F3 fish.

Fluorescence *in situ* hybridization

In situ hybridization was performed for *bmp6* and *sp7*, markers of osteoblasts in zebrafish. The tissue was fixed in 4% paraformaldehyde for 24 h, dehydrated using a series of gradient ethanol baths, embedded in paraffin, and sliced horizontally (5 μm). According to the coding sequences of *bmp6* and *sp7*, primers were designed (bmp6_F1:5′ TGCTGGAATCTCGCAGGTTG 3′, bmp6_R1:5′ TAATACGACTCACTATAGGGAGAGATGAGCCGGTCCCTTTGATG 3′; sp7_F1:5′ GACCCTCACTGGACTGCTTC 3′, sp7_R1:5′ TAATACGACTCACTATAGGGAGAGCGGCATTTGAGGATTGAGCG 3′). The PCR products were purified, and a DIG-tagged *bmp6* probe and a fluorescein-tagged *sp7* probe were synthesized. Dual fluorescence *in situ* hybridization was performed according to the method described by Fominaya et al. (2016). Two antibodies, anti-DIG-POD, Fab fragments (Roche Diagnostics GmbH, Shanghai, China) and anti-fluorescein-POD, Fab fragments (Roche Diagnostics GmbH), were used to bind the probes separately. Then, tyramide signal amplification (TSA) was used for chromogenic reaction with *bmp6* labeled in green and *sp7* labeled in red, and DAPI labeled in blue for nuclei (Figure S6 in Supporting Information).

Bone staining for *bmp6*$^{-/-}$ mutants

Mineralized bone was stained with Alizarin Red using the following modified protocol from the lab of P. Eckhard Witten in Ghent University (Belgium) for larvae and adult fish: (i) fix the specimens in 4% paraformaldehyde overnight; (ii) wash specimens thrice with 1% PBST (0.1% Tween 20), 5 min each time; (iii) prepare the bleach solution by mixing 3% H_2O_2 and 2% KOH according to a ratio of 1:2; (iv) add this bleach solution to the specimens and process the sample for 10 min (depending on the size of the specimens, this does not take a long time and has to be observed carefully) until the specimens is transparent; (v) wash specimens thrice with water, for 5 min each time; (vi) transfer the sample to Alizarin Red S (0.1%) for 1–2 h (depending on the size of the specimen, timing observation, adjusting the dyeing time); (vii) Wash thrice with water; (viii) place the sample in 50% glycerol-KOH to make them transparent, and then transfer to 70% before storing it in 100% glycerol for examination; (ix) The stained specimens were analyzed and photographed using an Olympus SZX2 stereo microscope (Japan).

Transcriptome analyses for *bmp6*$^{-/-}$ mutants

Total RNA was isolated from whole fish at 45 dpf wild type and mutants using RNAiso Plus Reagent (TaKaRa, Beijing, China). Subsequently, total RNA was quantified using a 2100 Bioanalyzer system (Agilent Technology, USA), and samples that met the quality requirements were used for RNA-seq library preparation. Three biological duplicates were used for wild-type and mutant lines, respectively, and a total of six libraries were generated and sequenced on an Illumina HiSeq platform. After quality control of the raw data, paired-end clean reads were aligned to the zebrafish reference genome (ftp://ftp.ensembl.org/pub/release-92/fasta/danio_rerio/). Then the FPKM of each gene was calculated, and differential expression analysis was performed using the DESeq R package (1.18.0) (Wang et al., 2010). Genes with a *P*-value<0.05 and a fold change of >2 or <0.5 were defined as differentially expressed genes (DEGs) after controlling for the false discovery rate (Figure S7 in Supporting Information).

Behavioral observation for *bmp6*$^{-/-}$ mutants

The methods were modified from those described by Yuan et al. (2021). Wild types and mutants (all 90 dpf) were sepa-

rately transferred to an experimental tank (length 30 cm ×height 24 cm×width 12 cm filled with 2 L of clean water) with a uniform cold white light source. The wild types and mutants were allowed to acclimatize to the environment for at least 1 h. A digital video format (Sony, Beijing, China) was used to record videos 10 min after the fish were acclimated to the environment, and EthoVision XT 14 software (Noldus Information Technology, Beijing, China) was used to analyze the behavioral changes (speed, swimming route, and reaction time) between the wild-type and mutant strains. The wild-type and mutants had six biological replicates. During all experiments, the room and water temperatures were maintained at 25°C±1°C.

Identification of chemosensory receptor families

We identified four chemosensory receptor families OR, TAAR, ORA/V1R and OlfC/V2R, in 17 teleosts (zebrafish, Atlantic cod, opah, fugu, stickleback, turbot, platyfish, medaka, bluefin tuna, Manado pipefish, Gulf pipefish, big-belly seahorse, lined seahorse, tiger tail seahorse, alligator pipefish, weedy seadragon, and leafy seadragon). First, we downloaded the OR, TAAR, ORA/V1R, and OlfC/V2R sequences of zebrafish, medaka, tilapia, and tiger-tail seahorse from public databases or published articles. These sequences were used as initial queries. A genome-wide survey was performed in leafy seadragon and other 16 teleosts using the Gene Model Mapper (GeMoMa) v1.7.1 (Keilwagen et al., 2016). Briefly, the module Extractor in GeMoMa was used to extract coding exons as queries. We selected mmseqs as the search algorithm to search for the target genome with query sequences. Module GeneModelMapper was used to build gene models from mmseqs search results. Module GAF was used to merge and filter the gene models by combining predictions from different reference organisms. Finally, the Annotation Finalizer module was used to rename the predictions. We only retrieved high-quality gene models with completeness (start==‘M’ and steo==‘*’) and high relative scores (score/aa≥1.5). Pseudogenes were predicted using Shiu Lab’s pseudogene pipeline (Campbell et al., 2014).

Phylogenetic analysis for chemosensory receptor families

For each of the four chemosensory receptor families, the amino acid sequences of all 17 species were aligned using MAFFT v7.475 (https://mafft.cbrc.jp/alignment/software/) with the default parameters. Then the alignments were manually adjusted to delete gaps with 90% tolerance. For phylogenetic analysis, ProteinModelSelection.pl provided with RAxML v8.2.12 (Stamatakis, 2014) was used to deduce the best-suited substitution model, and a tree was constructed using RAxML with BS (BootStrap) and ML search type. Subsequently, the tree topologies were rendered in FigTree v1.4.4.

Estimation of gene gain and loss of chemosensory receptor families

We estimated gene gain and loss for each of the four chemosensory receptor families. CAFE was used to reconstruct the phylogenetic history and infer copy numbers for all ancestral nodes using the identified complete genes. First, a text file containing the gene number of each subfamily for each species was prepared. Species trees with divergence times were obtained from our phylogenomic analysis. CAFE uses a birth and death process to model gene gain and loss across tree species. The *P*-value was set to 0.05. To calculate the gene gain and loss for each ancestral node in the species tree, copy numbers for all subfamilies in each node were counted.

Data availability

The raw data and genome assembly are available from the National Center for Biotechnology Information BioProject under the accession code PRJNA838714 and PRJNA842165.

Compliance and ethics *The authors declare that they have no conflict of interest. The procedures related to animal subjects of our study were approved by Ethic Committee of South China Sea Institute of Oceanology, Chinese Academy of Sciences.*

Acknowledgements *This work was supported by the National Natural Science Foundation of China (41825013, 42230409, 42006108, 42276126), Key Research Program of Frontier Sciences of CAS (ZDBS-LY-DQC004), the National Key Research and Development Program of China (2021YFF0502803), Strategic Priority Research Program of the Chinese Academy of Sciences (XDB42030204) and South China Sea Institute of Oceanology of the Chinese Academy of Sciences (SCSIO202208).*

References

Ahlberg, P.E. (2021). A comparative genomic framework for the fish-tetrapod transition. Sci China Life Sci 64, 664–666.

Ahuja, G., and Korsching, S. (2014). Zebrafish olfactory receptor ORA1 recognizes a putative reproductive pheromone. Commun Integr Biol 7, e970501.

Assis, J., Tyberghein, L., Bosch, S., Verbruggen, H., Serrão, E.A., De Clerck, O., and Tittensor, D. (2018). Bio-ORACLE v2.0: extending marine data layers for bioclimatic modelling. Glob Ecol Biogeogr 27, 277–284.

Bachmann, K., Patel, H., Batayneh, Z., Slama, J., White, D., Posey, J., Ekins, S., Gold, D., and Sambucetti, L. (2004). PXR and the regulation of apoA1 and HDL-cholesterol in rodents. Pharmacol Res 50, 237–246.

Benson, G. (1999). Tandem repeats finder: a program to analyze DNA sequences. Nucleic Acids Res 27, 573–580.

Bian, C., Hu, Y., Ravi, V., Kuznetsova, I.S., Shen, X., Mu, X., Sun, Y., You, X., Li, J., Li, X., et al. (2016). The Asian arowana (*Scleropages formosus*) genome provides new insights into the evolution of an early lineage of teleosts. Sci Rep 6, 24501.

Birney, E., Clamp, M., and Durbin, R. (2004). GeneWise and genomewise. Genome Res 14, 988–995.

Blonder, B., Morrow, C.B., Maitner, B., Harris, D.J., Lamanna, C., Violle, C., Enquist, B.J., and Kerkhoff, A.J. (2018). New approaches for delineating *n*-dimensional hypervolumes. Methods Ecol Evol 9, 305–319.

Branshaw, P. (2005). Leafy seadragon, *Phycodurus eques*. In: Koldewey, H.

J., ed. Syngnathid Husbandry in Public Aquariums Manual. London: Project Seahorse and the Zoological Society of London. 96–107.
Browne, R.K., Baker, J.L., and Connolly, R.M. (2008). Syngnathids: seadragons, seahorses, and pipefishes of Gulf St Vincent. In: Shepherd, S. A., Bryars, S., Kirkegaard, I.R., Harbison, P., and Jennings, J.T., eds. Natural History of Gulf St Vincent. Adelaide: The University of Adelaide, Royal Society of South Australia (Inc.) 162–176..
Campbell, D.S., and Okamoto, H. (2013). Local caspase activation interacts with Slit-Robo signaling to restrict axonal arborization. J Cell Biol 203, 657–672.
Campbell, M.A., Haas, B.J., Hamilton, J.P., Mount, S.M., and Buell, C.R. (2006). Comprehensive analysis of alternative splicing in rice and comparative analyses with *Arabidopsis*. BMC Genomics 7, 327.
Campbell, M.S., Law, M.Y., Holt, C., Stein, J.C., Moghe, G.D., Hufnagel, D.E., Lei, J., Achawanantakun, R., Jiao, D., Lawrence, C.J., et al. (2014). MAKER-P: a tool kit for the rapid creation, management, and quality control of plant genome annotations. Plant Physiol 164, 513–524.
Chaisson, M.J., and Tesler, G. (2012). Mapping single molecule sequencing reads using basic local alignment with successive refinement (BLASR): application and theory. BMC Bioinf 13, 1–8.
Chen, S., and Huang, X. (2020). DNA sequencing: the key to unveiling genome. Sci China Life Sci 63, 1593–1596.
Cheng, H., Concepcion, G.T., Feng, X., Zhang, H., and Li, H. (2021). Haplotype-resolved de novo assembly using phased assembly graphs with hifiasm. Nat Methods 18, 170–175.
Cheng, X.N., Shao, M., and Shi, D.L. (2018). Mutation of frizzled8a delays neural retinal cell differentiation and results in microphthalmia in zebrafish. Int J Dev Biol 62, 285–291.
Cong, X., Zheng, Q., Ren, W., Chéron, J.B., Fiorucci, S., Wen, T., Zhang, C., Yu, H., Golebiowski, J., and Yu, Y. (2019). Zebrafish olfactory receptors ORAs differentially detect bile acids and bile salts. J Biol Chem 294, 6762–6771.
Connolly, R.M., Melville, A.J., and Keesing, J.K. (2002). Abundance, movement and individual identification of leafy seadragons, *Phycodurus eques* (Pisces: Syngnathidae). Mar Freshwater Res 53, 777–780.
Darwin, C. (2004). On the Origin of Species, 1859. London: Routledge.
De Bie, T., Cristianini, N., Demuth, J.P., and Hahn, M.W. (2006). CAFE: a computational tool for the study of gene family evolution. Bioinformatics 22, 1269–1271.
Díaz, S.M., Settele, J., Brondízio, E., Ngo, H., Guèze, M., Agard, J., Arneth, A., Balvanera, P., Brauman, K., and Butchart, S. (2019). The global assessment report on biodiversity and ecosystem services: summary for policy makers. Available from: URL: https://ipbesnet/sites/default/files/2020-02/ipbes_global_assessment_report_summary_for_policymakers_enpdf.
Dobrowski, S.Z., Littlefield, C.E., Lyons, D.S., Hollenberg, C., Carroll, C., Parks, S.A., Abatzoglou, J.T., Hegewisch, K., and Gage, J. (2021). Protected-area targets could be undermined by climate change-driven shifts in ecoregions and biomes. Commun Earth Environ 2, 1.
Emms, D.M., and Kelly, S. (2015). OrthoFinder: solving fundamental biases in whole genome comparisons dramatically improves orthogroup inference accuracy. Genome Biol 16, 157.
Endo, S., Maeda, S., Matsunaga, T., Dhagat, U., El-Kabbani, O., Tanaka, N., Nakamura, K.T., Tajima, K., and Hara, A. (2009). Molecular determinants for the stereospecific reduction of 3-ketosteroids and reactivity towards all-trans-retinal of a short-chain dehydrogenase/reductase (DHRS4). Arch Biochem Biophys 481, 183–190.
Escher, G., Krozowski, Z., Croft, K.D., and Sviridov, D. (2003). Expression of sterol 27-hydroxylase (CYP27A1) enhances cholesterol efflux. J Biol Chem 278, 11015–11019.
Fominaya, A., Loarce, Y., González, J.M., and Ferrer, E. (2016). Tyramide signal amplification: fluorescence *in situ* hybridization for identifying homoeologous chromosomes. In: Kianian, S., and Kianian, P., eds. Plant Cytogenetics. Methods in Molecular Biology. New York: Humana Press. 35–48.
Froese, R., and Pauly, D. (2022). Fishbase, 2022. In World Wide Web electronic publication (update ver 02/2022).
Ge, S., and Guo, Y.L. (2020). Evolution of genes and genomes in the genomics era. Sci China Life Sci 63, 602–605.
Geng, F., Cheng, X., Wu, X., Yoo, J.Y., Cheng, C., Guo, J.Y., Mo, X., Ru, P., Hurwitz, B., Kim, S.H., et al. (2016). Inhibition of SOAT1 suppresses glioblastoma growth via blocking SREBP-1-mediated lipogenesis. Clin Cancer Res 22, 5337–5348.
Gnerre, S., MacCallum, I., Przybylski, D., Ribeiro, F.J., Burton, J.N., Walker, B.J., Sharpe, T., Hall, G., Shea, T.P., Sykes, S., et al. (2011). High-quality draft assemblies of mammalian genomes from massively parallel sequence data. Proc Natl Acad Sci USA 108, 1513–1518.
Groves, P. (1998). Leafy sea dragons. Sci Am 279, 84–89.
Guisan, A., Thuiller, W., and Zimmermann, N.E. (2017). Habitat Suitability and Distribution Models: with Applications in R. Cambridge: Cambridge University Press.
Gustafsen, C., Kjolby, M., Nyegaard, M., Mattheisen, M., Lundhede, J., Buttenschøn, H., Mors, O., Bentzon, J.F., Madsen, P., Nykjaer, A., et al. (2014). The hypercholesterolemia-risk gene *SORT1* facilitates PCSK9 secretion. Cell Metab 19, 310–318.
Haas, B.J., Salzberg, S.L., Zhu, W., Pertea, M., Allen, J.E., Orvis, J., White, O., Buell, C.R., and Wortman, J.R. (2008). Automated eukaryotic gene structure annotation using EVidenceModeler and the program to assemble spliced alignments. Genome Biol 9, R7.
Hamilton, H., Saarman, N., Short, G., Sellas, A.B., Moore, B., Hoang, T., Grace, C.L., Gomon, M., Crow, K., and Brian Simison, W. (2017). Molecular phylogeny and patterns of diversification in syngnathid fishes. Mol Phylogenet Evol 107, 388–403.
He, L., Long, X., Qi, J., Wang, Z., Huang, Z., Wu, S., Zhang, X., Luo, H., Chen, X., Lin, J., et al. (2021). Genome and gene evolution of seahorse species revealed by the chromosome-level genome of *Hippocampus abdominalis*. Mol Ecol Resour 22, 1465–1477.
Hu, J., Fan, J., Sun, Z., and Liu, S. (2020). NextPolish: a fast and efficient genome polishing tool for long-read assembly. Bioinformatics 36, 2253–2255.
Hu, Z.M., Zhang, Q.S., Zhang, J., Kass, J.M., Mammola, S., Fresia, P., Draisma, S.G.A., Assis, J., Jueterbock, A., Yokota, M., et al. (2021). Intraspecific genetic variation matters when predicting seagrass distribution under climate change. Mol Ecol 30, 3840–3855.
Hussain, A. (2011). The olfactory nervous system of terrestrial and aquatic vertebrates. Nat Prec doi: 10.1038/npre.2011.6642.1.
IUCN. (2020). IUCN 2021. IUCN Red List of Threatened Species. Version 2021-3.
Jiang, H., Du, K., Gan, X., Yang, L., and He, S. (2019). Massive loss of olfactory receptors but not trace amine-associated receptors in the world's deepest-living fish (*Pseudoliparis swirei*). Genes 10, 910.
Jones, P., Binns, D., Chang, H.Y., Fraser, M., Li, W., McAnulla, C., McWilliam, H., Maslen, J., Mitchell, A., Nuka, G., et al. (2014). InterProScan 5: genome-scale protein function classification. Bioinformatics 30, 1236–1240.
Kanehisa, M., and Goto, S. (2000). KEGG: Kyoto Encyclopedia of Genes and Genomes. Nucleic Acids Res 28, 27–30.
Karagic, N., Schneider, R.F., Meyer, A., and Hulsey, C.D. (2020). A genomic cluster containing novel and conserved genes is associated with cichlid fish dental developmental convergence. Mol Biol Evol 37, 3165–3174.
Kass, J.M., Muscarella, R., Galante, P.J., Bohl, C.L., Pinilla-Buitrago, G.E., Boria, R.A., Soley-Guardia, M., and Anderson, R.P. (2021). ENMeval 2.0: Redesigned for customizable and reproducible modeling of species' niches and distributions. Methods Ecol Evol 12, 1602–1608.
Keilwagen, J., Wenk, M., Erickson, J.L., Schattat, M.H., Grau, J., and Hartung, F. (2016). Using intron position conservation for homology-based gene prediction. Nucleic Acids Res 44, e89.
Kimura, T., Nagao, Y., Hashimoto, H., Yamamoto-Shiraishi, Y., Yamamoto, S., Yabe, T., Takada, S., Kinoshita, M., Kuroiwa, A., and Naruse, K. (2014). Leucophores are similar to xanthophores in their specification and differentiation processes in medaka. Proc Natl Acad Sci USA 111,

7343–7348.
Kolora, S.R.R., Owens, G.L., Vazquez, J.M., Stubbs, A., Chatla, K., Jainese, C., Seeto, K., McCrea, M., Sandel, M.W., Vianna, J.A., et al. (2021). Origins and evolution of extreme life span in Pacific Ocean rockfishes. Science 374, 842–847.
Korf, I. (2004). Gene finding in novel genomes. BMC Bioinf 5, 59.
Kramer-Schadt, S., Niedballa, J., Pilgrim, J.D., Schröder, B., Lindenborn, J., Reinfelder, V., Stillfried, M., Heckmann, I., Scharf, A.K., and Augeri, D.M. (2013). The importance of correcting for sampling bias in MaxEnt species distribution models. Divers Distrib 19, 1366–1379.
Kuiter, R.H. (2000). Seahorses and Their Relatives. New York: Twayne Publishers.
Li, C., Olave, M., Hou, Y., Qin, G., Schneider, R.F., Gao, Z., Tu, X., Wang, X., Qi, F., Nater, A., et al. (2021a). Genome sequences reveal global dispersal routes and suggest convergent genetic adaptations in seahorse evolution. Nat Commun 12, 1094.
Li, H. (2011). A statistical framework for SNP calling, mutation discovery, association mapping and population genetical parameter estimation from sequencing data. Bioinformatics 27, 2987–2993.
Li, H., and Durbin, R. (2009). Fast and accurate short read alignment with Burrows-Wheeler transform. Bioinformatics 25, 1754–1760.
Li, H., and Durbin, R. (2011). Inference of human population history from individual whole-genome sequences. Nature 475, 493–496.
Li, J., Bian, C., Yi, Y., Yu, H., You, X., and Shi, Q. (2021b). Temporal dynamics of teleost populations during the Pleistocene: a report from publicly available genome data. BMC Genomics 22, 490.
Li, Z., Chen, Y., Mu, D., Yuan, J., Shi, Y., Zhang, H., Gan, J., Li, N., Hu, X., Liu, B., et al. (2012). Comparison of the two major classes of assembly algorithms: overlap-layout-consensus and de-Bruijn-graph. Brief Funct Genomics 11, 25–37.
Lin, Q., Fan, S., Zhang, Y., Xu, M., Zhang, H., Yang, Y., Lee, A.P., Woltering, J.M., Ravi, V., Gunter, H.M., et al. (2016). The seahorse genome and the evolution of its specialized morphology. Nature 540, 395–399.
Lindsey, R., and Dahlman, L. (2020). Climate Change: Global Temperature. Science & Information for a Climate Smart-Nation. 1–5</r>.
Liu, H., Chen, C., Lv, M., Liu, N., Hu, Y., Zhang, H., Enbody, E.D., Gao, Z., Andersson, L., and Wang, W. (2021). A chromosome-level assembly of blunt snout bream (*Megalobrama amblycephala*) genome reveals an expansion of olfactory receptor genes in freshwater fish. Mol Biol Evol 38, 4238–4251.
Liu, W., Zhang, L., Xuan, K., Hu, C., Liu, S., Liao, L., Li, B., Jin, F., Shi, S., and Jin, Y. (2018). Alpl prevents bone ageing sensitivity by specifically regulating senescence and differentiation in mesenchymal stem cells. Bone Res 6, 1–5.
Lohbeck, K.T., Riebesell, U., and Reusch, T.B.H. (2012). Adaptive evolution of a key phytoplankton species to ocean acidification. Nat Geosci 5, 346–351.
Löytynoja, A. (2014). Phylogeny-aware alignment with PRANK. In: Russell, D., ed. Multiple Sequence Alignment Methods. Methods in Molecular Biology. Totowa: Humana Press. 155–170.
Lü, Z., Gong, L., Ren, Y., Chen, Y., Wang, Z., Liu, L., Li, H., Chen, X., Li, Z., Luo, H., et al. (2021). Large-scale sequencing of flatfish genomes provides insights into the polyphyletic origin of their specialized body plan. Nat Genet 53, 742–751.
Luu, P., Acher, F., Bertrand, H.O., Fan, J., and Ngai, J. (2004). Molecular determinants of ligand selectivity in a vertebrate odorant receptor. J Neurosci 24, 10128–10137.
Majoros, W.H., Pertea, M., and Salzberg, S.L. (2004). TigrScan and GlimmerHMM: two open source *ab initio* eukaryotic gene-finders. Bioinformatics 20, 2878–2879.
Manzini, I., and Korsching, S. (2011). The peripheral olfactory system of vertebrates: molecular, structural and functional basics of the sense of smell. e-Neuroforum 17, 68–77.
Melo-Merino, S.M., Reyes-Bonilla, H., and Lira-Noriega, A. (2020). Ecological niche models and species distribution models in marine environments: A literature review and spatial analysis of evidence. Ecol Model 415, 108837.
Mombaerts, P. (2004). Genes and ligands for odorant, vomeronasal and taste receptors. Nat Rev Neurosci 5, 263–278.
Moreno-Mateos, M.A., Vejnar, C.E., Beaudoin, J.D., Fernandez, J.P., Mis, E.K., Khokha, M.K., and Giraldez, A.J. (2015). CRISPRscan: designing highly efficient sgRNAs for CRISPR-Cas9 targeting *in vivo*. Nat Methods 12, 982–988.
Myers, E.W. (2005). The fragment assembly string graph. Bioinformatics 21, ii79–ii85.
Nikaido, M., Suzuki, H., Toyoda, A., Fujiyama, A., Hagino-Yamagishi, K., Kocher, T.D., Carleton, K., and Okada, N. (2013). Lineage-specific expansion of vomeronasal type 2 receptor-like (*OlfC*) genes in cichlids may contribute to diversification of amino acid detection systems. Genome Biol Evol 5, 711–722.
Nummela, S., Pihlström, H., Puolamäki, K., Fortelius, M., Hemilä, S., and Reuter, T. (2013). Exploring the mammalian sensory space: co-operations and trade-offs among senses. J Comp Physiol A 199, 1077–1092.
Ohlebusch, B., Borst, A., Frankenbach, T., Klopocki, E., Jakob, F., Liedtke, D., and Graser, S. (2020). Investigation of *alpl* expression and Tnap-activity in zebrafish implies conserved functions during skeletal and neuronal development. Sci Rep 10, 1–6.
Oram, J.F., and Lawn, R.M. (2001). ABCA1: the gatekeeper for eliminating excess tissue cholesterol. J Lipid Res 42, 1173–1179.
Paridaen, J.T.M.L., Janson, E., Utami, K.H., Pereboom, T.C., Essers, P.B., van Rooijen, C., Zivkovic, D., and MacInnes, A.W. (2011). The nucleolar GTP-binding proteins Gnl2 and nucleostemin are required for retinal neurogenesis in developing zebrafish. Dev Biol 355, 286–301.
Pollom, R.A., Ralph, G.M., Pollock, C.M., and Vincent, A.C.J. (2021). Global extinction risk for seahorses, pipefishes and their near relatives (Syngnathiformes). Oryx 55, 497–506.
Pullinger, C.R., Eng, C., Salen, G., Shefer, S., Batta, A.K., Erickson, S.K., Verhagen, A., Rivera, C.R., Mulvihill, S.J., Malloy, M.J., et al. (2002). Human cholesterol 7α-hydroxylase (CYP7A1) deficiency has a hypercholesterolemic phenotype. J Clin Invest 110, 109–117.
Qu, M., Liu, Y., Zhang, Y., Wan, S., Ravi, V., Qin, G., Jiang, H., Wang, X., Zhang, H., Zhang, B., et al. (2021). Seadragon genome analysis provides insights into its phenotype and sex determination locus. Sci Adv 7, eabg5196.
Quinlan, A.R., and Hall, I.M. (2010). BEDTools: a flexible suite of utilities for comparing genomic features. Bioinformatics 26, 841–842.
Sala, O.E., Stuart Chapin, F., Iii, F., Armesto, J.J., Berlow, E., Bloomfield, J., Dirzo, R., Huber-Sanwald, E., Huenneke, L.F., Jackson, R.B., et al. (2000). Global biodiversity scenarios for the year 2100. Science 287, 1770–1774.
Santaquiteria, A., Siqueira, A.C., Duarte-Ribeiro, E., Carnevale, G., White, W., Pogonoski, J., Baldwin, C.C., Ortí, G., Arcila, D., and Betancur, R. R. (2021). Phylogenomics and historical biogeography of seahorses, dragonets, goatfishes, and allies (Teleostei: Syngnatharia): assessing factors driving uncertainty in biogeographic inferences. Syst Biol 70, 1145–1162.
Santoriello, C., Gennaro, E., Anelli, V., Distel, M., Kelly, A., Köster, R.W., Hurlstone, A., and Mione, M. (2010). Kita driven expression of oncogenic HRAS leads to early onset and highly penetrant melanoma in zebrafish. PloS ONE *5*, e15170.
Savvaki, M., Kafetzis, G., Kaplanis, S.I., Ktena, N., Theodorakis, K., and Karagogeos, D. (2021). Neuronal, but not glial, Contactin 2 negatively regulates axon regeneration in the injured adult optic nerve. Eur J Neurosci 53, 1705–1721.
Sbrocco, E.J., and Barber, P.H. (2013). MARSPEC: ocean climate layers for marine spatial ecology. Ecology 94, 979.
Schiffels, S., and Durbin, R. (2014). Inferring human population size and separation history from multiple genome sequences. Nat Genet 46, 919–925.
Shepherd, B., Wandell, M., and Ross, R. (2017). Mating, birth, larval development and settlement of Bargibant's pygmy seahorse, *Hippocampus bargibanti* (Syngnathidae), in aquaria. AACL Bioflux 10,

1049–1063.
Sheridan, J.A., and Bickford, D. (2011). Shrinking body size as an ecological response to climate change. Nat Clim Change 1, 401–406.
Silva, L., and Antunes, A. (2017). Vomeronasal receptors in vertebrates and the evolution of pheromone detection. Annu Rev Anim Biosci 5, 353–370.
Simão, F.A., Waterhouse, R.M., Ioannidis, P., Kriventseva, E.V., and Zdobnov, E.M. (2015). BUSCO: assessing genome assembly and annotation completeness with single-copy orthologs. Bioinformatics 31, 3210–3212.
Small, C.M., Bassham, S., Catchen, J., Amores, A., Fuiten, A.M., Brown, R.S., Jones, A.G., and Cresko, W.A. (2016). The genome of the Gulf pipefish enables understanding of evolutionary innovations. Genome Biol 17, 258.
Small, C.M., Healey, H.M., Currey, M.C., Beck, E.A., Catchen, J., Lin, A. S.P., Cresko, W.A., and Bassham, S. (2022). Leafy and weedy seadragon genomes connect genic and repetitive DNA features to the extravagant biology of syngnathid fishes. Proc Natl Acad Sci USA 119, e2119602119.
Stamatakis, A. (2014). RAxML version 8: a tool for phylogenetic analysis and post-analysis of large phylogenies. Bioinformatics 30, 1312–1313.
Stanke, M., and Waack, S. (2003). Gene prediction with a hidden Markov model and a new intron submodel. Bioinformatics 19, ii215–ii225.
Stiller, J., da Fonseca, R.R., Alfaro, M.E., Faircloth, B.C., Wilson, N.G., and Rouse, G.W. (2021). Using ultraconserved elements to track the influence of sea-level change on leafy seadragon populations. Mol Ecol 30, 1364–1380.
Stiller, J., Short, G., Hamilton, H., Saarman, N., Longo, S., Wainwright, P., Rouse, G.W., and Simison, W.B. (2022). Phylogenomic analysis of Syngnathidae reveals novel relationships, origins of endemic diversity and variable diversification rates. BMC Biol 20, 1–2.
Stiller, J., Wilson, N.G., Donnellan, S., and Rouse, G.W. (2016). The leafy seadragon, *Phycodurus eques*, a flagship species with low but structured genetic variability. J Hered 108, 152–162.
Stiller, J., Wilson, N.G., and Rouse, G.W. (2015). A spectacular new species of seadragon (Syngnathidae). R Soc open sci 2, 140458.
Suda, A., Nishiki, I., Iwasaki, Y., Matsuura, A., Akita, T., Suzuki, N., and Fujiwara, A. (2019). Improvement of the Pacific bluefin tuna (*Thunnus orientalis*) reference genome and development of male-specific DNA markers. Sci Rep 9, 14450.
Tang, S., Lomsadze, A., and Borodovsky, M. (2015). Identification of protein coding regions in RNA transcripts. Nucleic Acids Res 43, e78.
Tarailo-Graovac, M., and Chen, N. (2009). Using RepeatMasker to identify repetitive elements in genomic sequences. Curr Protoc Bioinf 25.
Telgársky, R. (2014). Eyes, optics and imaging: mathematics and engineering innovations inspired by nature. Sci Issue Jan Długosz Univ Częstochowa Math 19.
Teske, P.R., and Beheregaray, L.B. (2009). Evolution of seahorses′ upright posture was linked to Oligocene expansion of seagrass habitats. Biol Lett 5, 521–523.
Thompson, A., Di, A.E., Sarwar, N., Erqou, S., Saleheen, D., Dullaart, R.P., Keavney, B., Ye, Z., and Danesh, J. (2008). Association of cholesteryl ester transfer protein genotypes with CETP mass and activity, lipid levels, and coronary risk. JAMA 299, 2777–2788.
Tørresen, O.K., Star, B., Jentoft, S., Reinar, W.B., Grove, H., Miller, J.R., Walenz, B.P., Knight, J., Ekholm, J.M., Peluso, P., et al. (2017). An improved genome assembly uncovers prolific tandem repeats in Atlantic cod. BMC Genomics 18, 95.
van Wassenbergh, S., Roos, G., and Ferry, L. (2011). An adaptive explanation for the horse-like shape of seahorses. Nat Commun 2, 164.
Vergés, A., Doropoulos, C., Malcolm, H.A., Skye, M., Garcia-Pizá, M., Marzinelli, E.M., Campbell, A.H., Ballesteros, E., Hoey, A.S., Vila-Concejo, A., et al. (2016). Long-term empirical evidence of ocean warming leading to tropicalization of fish communities, increased herbivory, and loss of kelp. Proc Natl Acad Sci USA 113, 13791–13796.
Walkiewicz, K., Benitez Cardenas, A.S., Sun, C., Bacorn, C., Saxer, G., and Shamoo, Y. (2012). Small changes in enzyme function can lead to surprisingly large fitness effects during adaptive evolution of antibiotic resistance. Proc Natl Acad Sci USA 109, 21408–21413.
Wang, L., Feng, Z., Wang, X., Wang, X., and Zhang, X. (2010). DEGseq: an R package for identifying differentially expressed genes from RNA-seq data. Bioinformatics 26, 136–138.
Wang, X., Qu, M., Liu, Y., Schneider, R.F., Song, Y., Chen, Z., Zhang, H., Zhang, Y., Yu, H., Zhang, S., et al. (2022). Genomic basis of evolutionary adaptation in a warm-blooded fish. Innovation 3, 100185.
Wang, X., and Wang, L. (2016). GMATA: an integrated software package for genome-scale SSR mining, marker development and viewing. Front Plant Sci 7.
Weber, J.A., Park, S.G., Luria, V., Jeon, S., Kim, H.M., Jeon, Y., Bhak, Y., Jun, J.H., Kim, S.W., Hong, W.H., et al. (2020). The whale shark genome reveals how genomic and physiological properties scale with body size. Proc Natl Acad Sci USA 117, 20662–20671.
Wei, F., Huang, G., Guan, D., Fan, H., Zhou, W., Wang, D., and Hu, Y. (2022). Digital Noah's Ark: last chance to save the endangered species. Sci China Life Sci 65, 2325–2327.
Wei, F. (2020). A new era for evolutionary developmental biology in non-model organisms. Sci China Life Sci 63, 1251–1253.
Wilson, N.G., Stiller, J., and Rouse, G.W. (2017). Barriers to gene flow in common seadragons (Syngnathidae: *Phyllopteryx taeniolatus*). Conserv Genet 18, 53–66.
Xiao, J., Lin, Z., Qin, H., Zheng, Z., Gong, F., Liu, Y., Li, X., and Fu, X. (2020). Growth factor regulatory system: a new system for not truly recognized organisms. Sci China Life Sci 63, 443–446.
Xu, H., Tong, G., Yan, T., Dong, L., Yang, X., Dou, D., Sun, Z., Liu, T., Zheng, X., Yang, J., et al. (2022). Transcriptomic analysis provides insights to reveal the *bmp6* function related to the development of intermuscular bones in zebrafish. Front Cell Dev Biol 10, 821471.
Xu, Z., and Wang, H. (2007). LTR_FINDER: an efficient tool for the prediction of full-length LTR retrotransposons. Nucleic Acids Res 35, W265–W268.
Yang, Z. (2007). PAML 4: phylogenetic analysis by maximum likelihood. Mol Biol Evol 24, 1586–1591.
Yarosh, W., Monserrate, J., Tong, J.J., Tse, S., Le, P.K., Nguyen, K., Brachmann, C.B., Wallace, D.C., and Huang, T. (2008). The molecular mechanisms of OPA1-mediated optic atrophy in *Drosophila* model and prospects for antioxidant treatment. PLoS Genet 4, e6.
Yuan, S., Liang, C., Li, W., Letcher, R.J., and Liu, C. (2021). A comprehensive system for detection of behavioral change of *D. magna* exposed to various chemicals. J Hazard Mater 402, 123731.
Zapilko, V., and Korsching, S.I. (2016). Tetrapod V1R-like *ora* genes in an early-diverging ray-finned fish species: the canonical six *ora* gene repertoire of teleost fish resulted from gene loss in a larger ancestral repertoire. BMC Genomics 17, 83.
Zhang, Y.H., Ravi, V., Qin, G., Dai, H., Zhang, H.X., Han, F.M., Wang, X., Liu, Y.H., Yin, J.P., Huang, L.M., et al. (2020). Comparative genomics reveal shared genomic changes in syngnathid fishes and signatures of genetic convergence with placental mammals. Natl Sci Rev 7, 964–977.